

ARTICLE OPEN



Simultaneous inhibition of PI3K and PAK in preclinical models of neurofibromatosis type 2-related schwannomatosis

Anna Nagel ^{1,2}, Julianne Huegel ^{1,2}, Alejandra Petrilli ¹, Rosa Rosario¹, Berta Victoria¹, Haley M Hardin ¹ and Cristina Fernandez-Valle ¹✉

© The Author(s) 2024

Neurofibromatosis Type 2 (NF2)-related schwannomatosis is a genetic disorder that causes development of multiple types of nervous system tumors. The primary and diagnostic tumor type is bilateral vestibular schwannoma. There is no cure or drug therapy for NF2. Recommended treatments include surgical resection and radiation, both of which can leave patients with severe neurological deficits or increase the risk of future malignant tumors. Results of our previous pilot high-throughput drug screen identified phosphoinositide 3-kinase (PI3K) inhibitors as strong candidates based on loss of viability of mouse merlin-deficient Schwann cells (MD-SCs). Here we used novel human schwannoma model cells to conduct combination drug screens. We identified a class I PI3K inhibitor, pictilisib and p21 activated kinase (PAK) inhibitor, PF-3758309 as the top combination due to high synergy in cell viability assays. Both single and combination therapies significantly reduced growth of mouse MD-SCs in an orthotopic allograft mouse model. The inhibitor combination promoted cell cycle arrest and apoptosis in mouse merlin-deficient Schwann (MD-SCs) cells and cell cycle arrest in human MD-SCs. This study identifies the PI3K and PAK pathways as potential targets for combination drug treatment of NF2-related schwannomatosis.

Oncogene (2024) 43:921–930; <https://doi.org/10.1038/s41388-024-02958-w>

INTRODUCTION

Neurofibromatosis Type 2 (NF2)-related schwannomatosis is a rare autosomal dominant disorder that causes formation of multiple tumor types in the nervous system [1]. Although the primary and diagnostic tumor type is bilateral vestibular schwannoma, patients simultaneously develop other schwannomas, meningiomas, and ependymomas [2]. Pathogenic variants in *NF2* inactivate the merlin tumor suppressor, a scaffold protein controlling downstream signaling from numerous cell surface receptors that stimulate Schwann cell proliferation and/or survival [3, 4]. Individuals with NF2 undergo regular monitoring and tumors are treated, when necessary, with surgery, radiation, or experimental drug therapies [5–7]. There is a great need for an effective and well-tolerated drug therapy for this patient population.

NF2 pathogenic variants have been identified in spontaneously occurring schwannomas and meningiomas, as well as many types of cancer including mesothelioma, glioma multiforme, breast, colorectal, skin, hepatic and prostate [8–10]. Population studies suggest that tumors with sporadic *NF2* mutations could occur in up to 1 in 300 people [11]. Although the role of merlin inactivation has not been well characterized in these other cancers, *NF2* status may be relevant for prognosis and future chemotherapeutic approaches.

Among the many merlin-dependent signaling pathways that control Schwann cell proliferation and survival is the PI3K pathway

where merlin was demonstrated to bind the PI3K enhancer PIKE-L to inhibit PI3K signaling [8]. Our previous pilot high-throughput screening study identified PI3K inhibitors as drug candidates based on their efficacy to reduce viability of mouse merlin-deficient Schwann cells [12]. Preliminary screening of 193 compounds alone and in combination has been conducted on our mouse and human merlin-deficient Schwann cells by the SYNODOS Consortium. Multiple PI3K inhibitors met criteria for efficacy and/or synergy [13, 14]. Although targeted single agent chemotherapeutics can inhibit tumor growth, drug resistance is common due to activation of alternative signaling pathways that sustain cell survival and proliferation [15, 16]. The purpose of this study was to identify drug combinations that co-targeted the PI3K pathway and secondary pathways using cell-based high-throughput screens and to confirm the efficacy of the most successful combination in an NF2-specific animal model.

Utilizing a synergistic drug screening approach, we identified a novel drug combination targeting PI3K and P21-associated kinase (PAK), confirmed its efficacy in an animal model of NF2-related schwannomatosis, and explored the mechanism through which these inhibitors decreased mouse and human MD-SCs proliferation and survival. Moreover, by identifying known merlin interactors as drug targets for schwannomas, we confirm the utility of our screening strategy and human schwannoma model cell lines for future identification of novel targets.

¹Burnett School of Biomedical Sciences, College of Medicine, University of Central Florida, Orlando, FL 32827, USA. ²These authors contributed equally: Anna Nagel, Julianne Huegel. ✉email: cfv@ucf.edu

Received: 2 October 2023 Revised: 19 January 2024 Accepted: 25 January 2024
Published online: 9 February 2024

RESULTS

Schwannoma model cells demonstrate loss of viability with co-inhibition of PI3K and several parallel/intersecting signaling pathways

The PI3K/Akt pathway inhibitor combinations and their targets evaluated in this study are shown in Table S1. The EC₅₀ of each agent tested as a monotherapy in five human and one mouse MD-SCs cell lines is presented in Table S2. Synergistic activity of drug combinations on MD-SC viability is summarized in Table S3 and Fig. S1. The most active single agent in the MD-SC is omipalisib, with an EC₅₀ of 2 nM in human MD-SCs. Synergy of was calculated using the Loewe Additivity model. Targeted co-inhibition of PI3K and PAK using pictilisib and PF-3758309 respectively induced the most synergistic loss of cell viability across three human MD-SC lines and one mouse MD-SC line (Table S3, Supplementary Fig. S1).

Dose response results in human MD-SC: primary HS01 engineered by shRNA knockdown of merlin (isogenic normal primary HS11) and HS03 engineered by CRISPR/Cas9 deletion of *NF2* (isogenic normal primary HS13) demonstrate loss of cell viability with single drug treatments (Fig. 1A, D) and at much lower concentrations with combination drug treatment (Fig. 1B, E). Loewe synergy scores for each drug concentration combination (10 × 10) show consistent synergy in human MD-SCs (Fig. 1C, F). Identical screening experiments performed in mouse MD-SCs shows similar inhibitory effects of single drugs (Fig. 1G) and combination treatment (Fig. 1H). Patterns of combined treatment synergy remained consistent in mouse cells (Fig. 1I).

Pictilisib and PF-3558309 have different pharmacokinetic profiles alone and in combination

Blood and sciatic nerve samples were collected from mice at 1, 2, 4, 8, and 24 h after a single oral gavage of pictilisib and PF-3758309 individually and combined. Pictilisib, when administered as a single agent, was rapidly absorbed, and distributed in both plasma and nerve (Supplementary Fig. S2A). Pictilisib penetrated the normal blood-nerve barrier (BNB), and the intraneural concentration had a longer half-life than in plasma (Supplementary Fig. S2C). Maximum plasma and nerve concentrations were reached at 1 h. In contrast, PF-3758309 was not detected in the intact nerve indicating it was impermeable to the BNB, had a shorter half-life in plasma than pictilisib, and reached a maximum plasma level at 2 h post oral gavage (Supplementary Fig. S2 B, C). When pictilisib and PF-3758309 were co-administered, the half-life of pictilisib in plasma greatly increased compared to the monotherapy half-life ($t_{1/2}$ 23.1 h vs 4.97 h, respectively, Supplementary Fig. S2D). In contrast, its half-life in nerve decreased ($t_{1/2}$ 7 h vs 16.51 h, Supplementary Fig. S2F). The calculated half-life of PF-3758309 in plasma when administered together with pictilisib or alone was similar. However, the maximum concentration in plasma increased three-fold when co-administered with pictilisib (341 vs 110 ng/ml). PF-3758309 remained undetected in normal nerve when co-administered with pictilisib (Supplementary Fig. S2E). These differences support a drug-drug interaction in vivo.

Combinatorial PI3K/PAK inhibition decreases orthotopic MD-MSc allograft growth rate and size

To evaluate the efficacy of pictilisib and PF-3758309 in vivo, sciatic nerves of NSG mice were grafted with 5,000 luciferase-expressing MD-MSCs and tumors were allowed to form for 1 week. Following 2 weeks of treatment, tumors were excised from euthanized mice. Three animals from each group were assigned for pharmacokinetic analysis, from which plasma and contralateral control (uninjected) sciatic nerves were also collected and assessed for drug concentration in each tissue at the time of euthanasia. Concentrations of drugs were similar to those found in the initial pharmacokinetic study for plasma

and nerve at 4 h post-gavage (Supplementary Fig. S3). However, we additionally measured the concentration of each inhibitor in the tumor, demonstrating that PF-3758309 is in fact bioavailable in the tumor despite not being detected in uninjected nerves. This suggests that the tumor neovasculature differs from that of the control nerve, and that the BNB is disrupted after nerves are grafted with merlin-deficient Schwann cells.

IVIS bioluminescent data and images demonstrate decreased rates of tumor growth with both PF-3758309 and combination treatments when assessing IVIS fold change over the treatment time course (Fig. 2A, C) All excised tumors were weighed prior to processing for pharmacokinetics or histology. Tumor weight was significantly decreased in pictilisib, and combination treated groups compared to controls (Fig. 2B).

Combinatorial PI3K/PAK inhibition reduces cell proliferation, increases apoptosis, and reduces Akt phosphorylation and YAP expression in vivo

To evaluate specific effects of PI3K and PAK inhibition in vivo, tumors ($n=4$ /group) were processed for immunohistological analysis. Images of H&E-stained sections from each tumor are shown at low magnification in Supplementary Fig. S4A; tumors were unique in size and shape and display regions of tissue heterogeneity. S100 was used as a marker of Schwann cells to detect grafted cells within the tumor. There were no clear differences in S100 staining patterns across groups (Supplementary Fig. S4B); this was confirmed with positive staining quantification ($p=0.86$, data not shown). Ki67 staining and quantification demonstrate significantly decreased cell proliferation in PF-3758309 and combination treated groups (Fig. 2D, E). Expression of cleaved caspase 3 was increased in pictilisib and combination treated groups (Fig. 2D, E), suggesting activation of apoptotic cell death. We were unable to confirm regulation of PAK signaling, as pPAK levels were similar across control and all treatment groups (Fig. 3D, E). Additionally, inhibition of PI3K signaling as measured by pAkt levels was only significant in combination treated samples (Fig. 2E). Because targeted pathways were not clearly inhibited with single treatments as expected, we assessed YAP as a downstream regulator of cell survival. Vehicle treated tumors stained intensely for YAP expression. Interestingly, all treatments decreased YAP staining; reduction with PF-3758309 and combination treatments were statistically significant (Fig. 2E).

Neither PI3K nor PAK inhibitor affect normal morphology of contralateral control nerve

Although only pictilisib can penetrate intact nerves, we assessed contralateral sciatic nerves with immunohistochemistry to qualitatively assess Schwann cell and neuron structure and morphology after exposure to the inhibitors. We were not able to distinguish differences in patterns of H&E staining or localized expression of myelin protein zero or neurofilaments (Supplementary Fig. S5).

Combinatorial PI3K/PAK inhibition induces synergistic cell cycle arrest in human MD-SCs and mouse MD-SCs

To assess the mechanism of loss of cell viability with both pictilisib and PF-3758309, human MD-SCs were treated with single and combination drugs at EC₅₀ concentrations. After 24 h of single drug treatment, there were significantly more HS01 cells in G1 phase and significantly fewer cells in S phase (Fig. 3A, B, Supplementary Fig. S6). Combinatorial treatment led to significantly larger G1 and smaller S phase populations than either single treatment. This was confirmed in a 72 h time course study assessing cell confluence and cleaved caspase 3/7-positive (CC3/7+) cells. Both single treatments led to decreased cell confluence compared to DMSO controls starting at 6 h of treatment (Fig. 3C, top). Combination treated cells also demonstrated significantly lower cell confluence from both

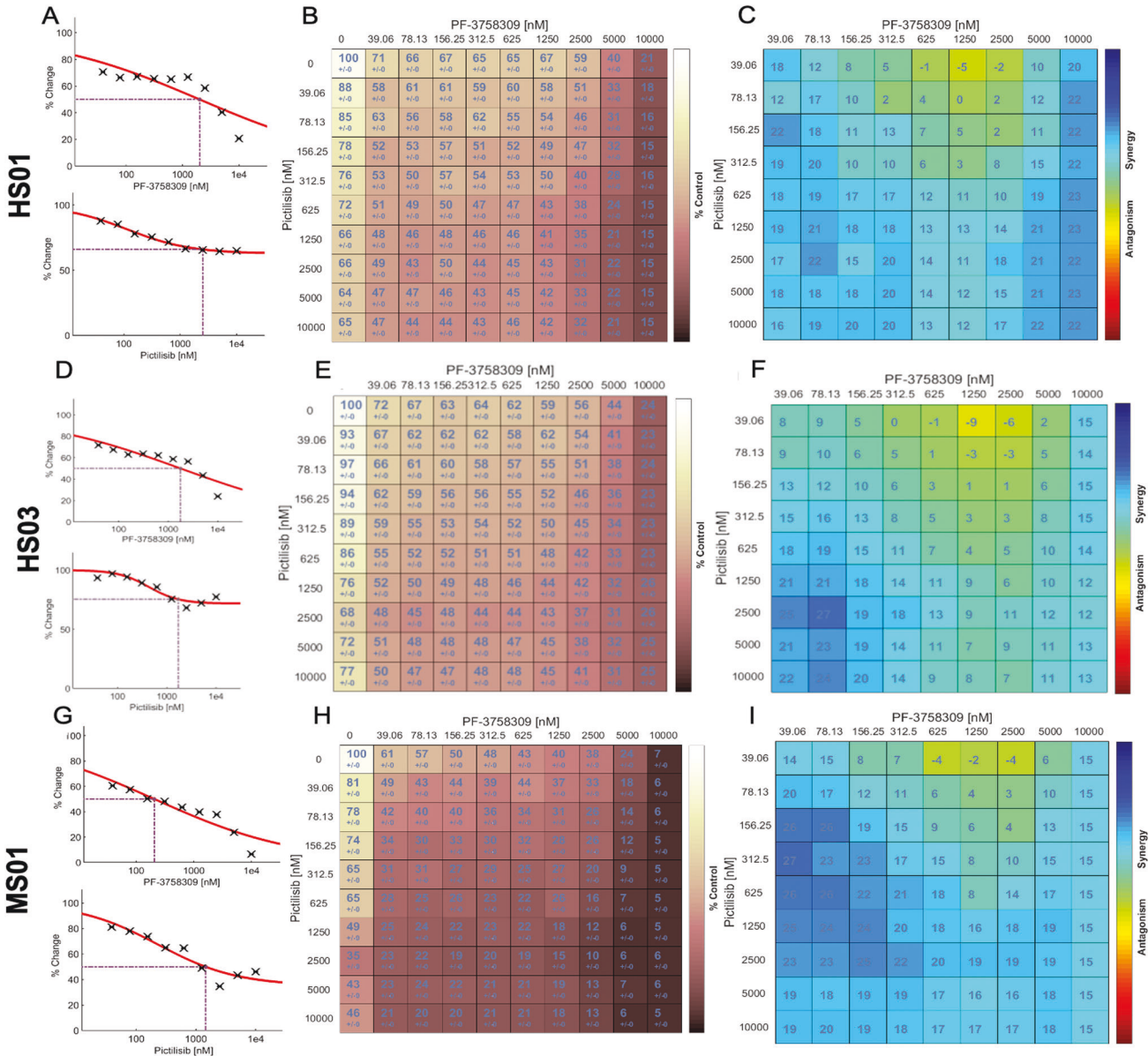
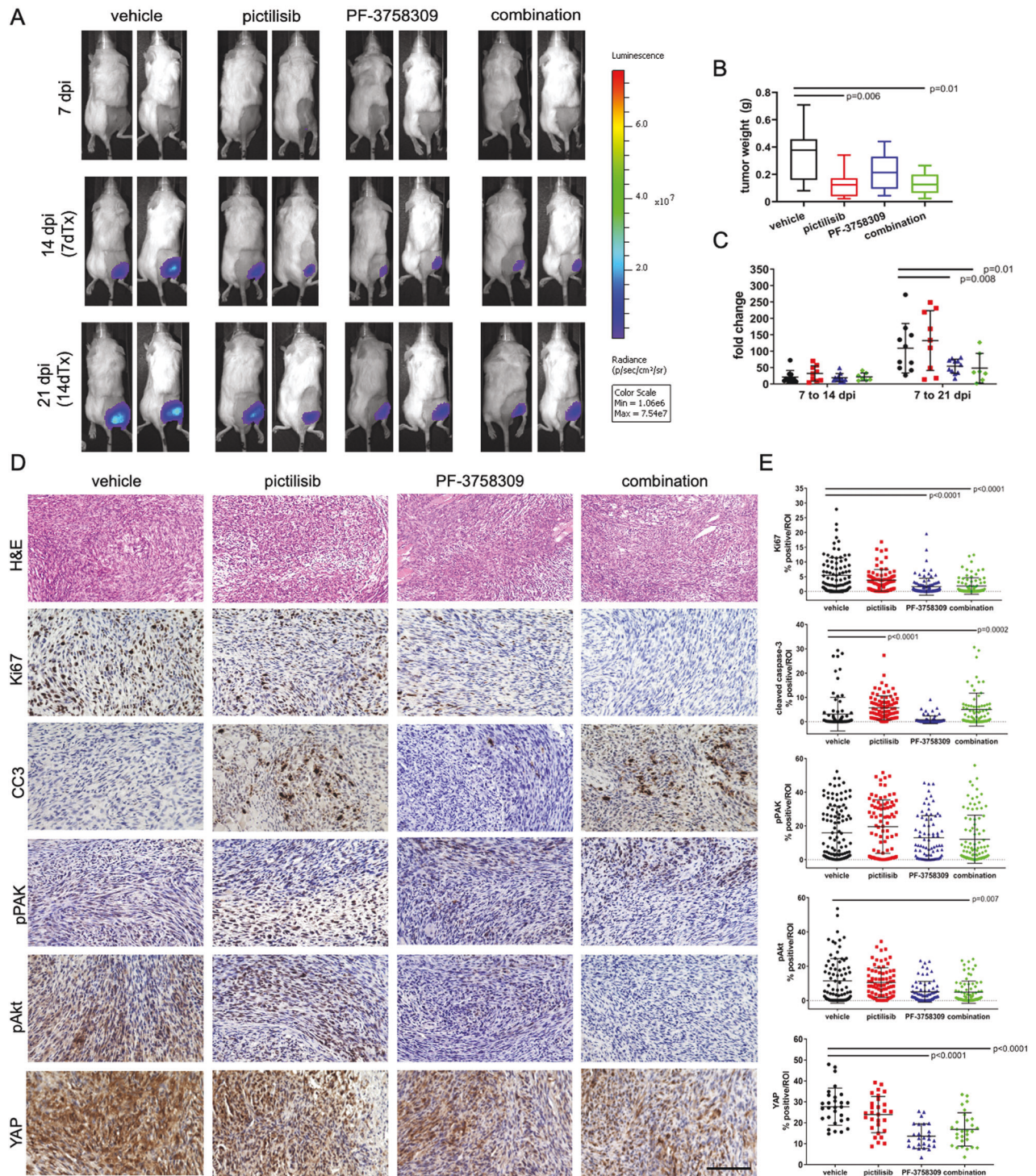


Fig. 1 Combinatorial PI3K/PAK inhibition synergistically decreases MD-SC viability. Screening results from human MD-SCs demonstrate loss of HS01 and HS03 cells viability with single drug treatments (A and D, EC50 or ECmax indicated with dotted line), with combination drug treatment (B, E), and synergy scores for each pair of combination treatments after 72 h (C, F). Similar screening performed on mouse MD-SCs shows loss of MS01 viability with single drug treatments (G), with combination drug treatment (H), and Loewe synergy scores for each pair of combination treatments after 48 h (I). In (B, E, H) color scale indicates loss of cell viability (light = high viability, dark = low viability) and numbers indicate percent of control cell viability. In (C, F, E) color scale indicates synergy (blue = synergy, red = antagonism) and numbers indicate percent difference in loss of viability compared to expected values (assuming no synergy).

control (starting at 6 h) and single drug-treated cells (starting at 44 h). Neither of the single drugs induced CC3/7 cleavage alone, however the combination induced low levels of CC3/7 (Fig. 3C, bottom). CUDC907 was used as a positive control for cleaved caspase 3/7-dependent apoptosis (high CC-3/7 signal starting at 14 h). Representative images from several time points are shown in Supplementary Fig. S7.

Since we observed a higher cleaved caspase-3 (CC-3) signal after pictilisib treatment in the mouse model, we decided to compare human (HS02) and mouse (MS01) MD-SCs cells in vitro using a previously described Incucyte CC-3/7 assay [14]. Human MD-SC lines exhibited significantly reduced confluency after pictilisib treatment (Fig. 4A), however no cleaved caspase-3/7 signal was detected (Fig. 4B), suggesting that pictilisib affects

cell cycle but does not induce apoptosis in human MD-SCs. In contrast, mouse MD-SCs exhibited low confluency and a high CC-3/7 signal after pictilisib treatment (Fig. 4A, B). CUDC907 was used as a positive control for apoptosis. To further analyze the differences between the cell lines, we performed human and mouse apoptotic protein arrays (Fig. 4C–F). Human arrays showed no difference in CC-3, anti-apoptotic proteins like Bcl-2 and Bcl-x, and significant increase in XIAP between vehicle and pictilisib-treated HS02 (Fig. 4D, F). In contrast, the mouse array showed a significant increase in CC-3 after pictilisib treatment, as well as a significant decrease in anti-apoptotic proteins Bcl-2, Bcl-x and XIAP compared to vehicle in MS01 cells (Fig. 4E, F). These results suggests that human and mouse MD-SCs respond differently to PI3K inhibition.



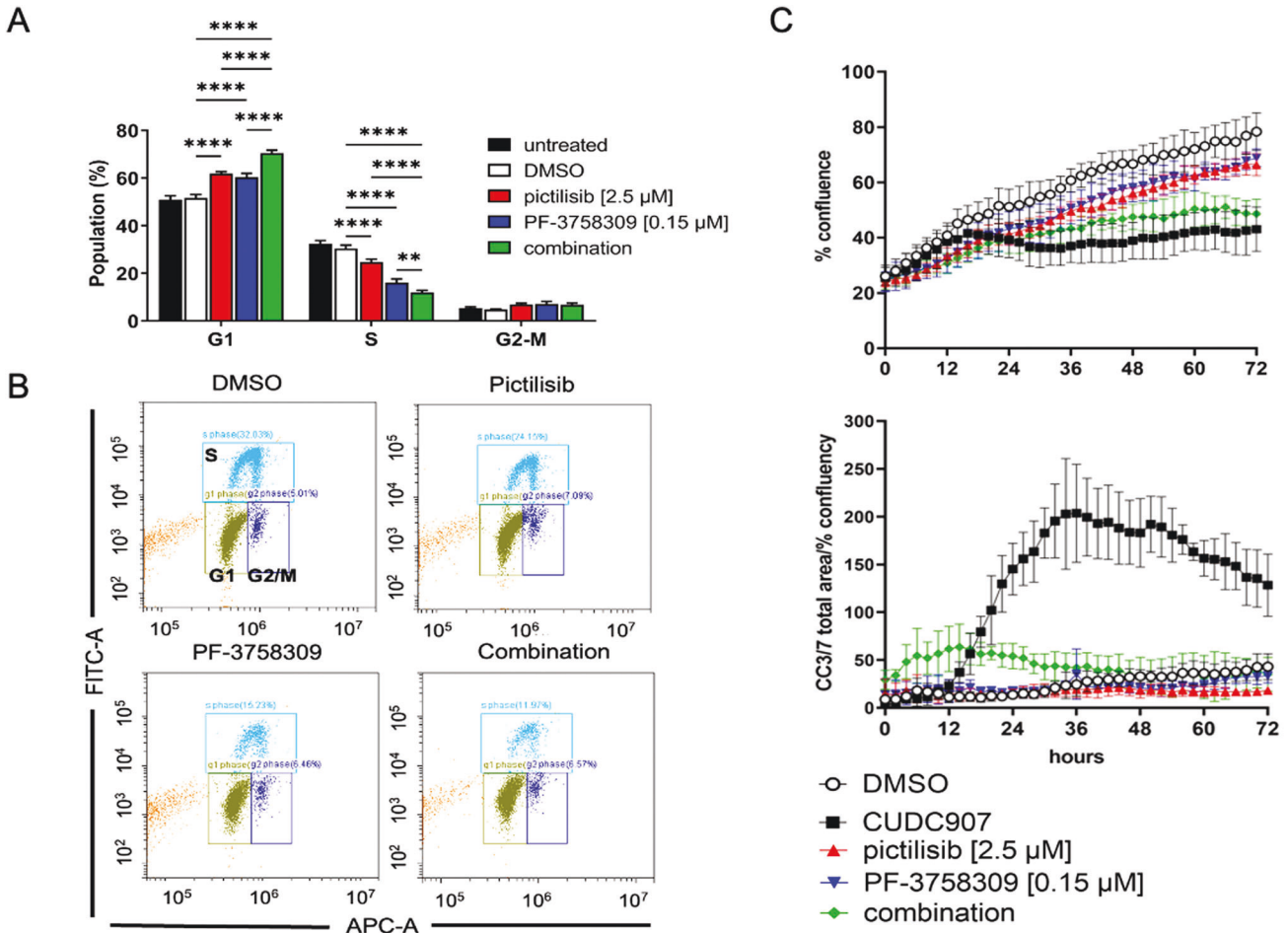


Fig. 3 Combinatorial PI3K/PAK inhibition arrests human MD-SC at the G1 phase of the cell cycle. **A** Graph of the distribution of cell cycle phases (gated for the live population) of all experimental runs as mean \pm SD. $**p < 0.01$, $***p < 0.001$, $****p < 0.0001$ (**B**). Representative plots of the distribution of FITC (EdU) and FxCycle (DNA content)-labeled cells of 0.001% DMSO vehicle control and drug-treated cells. **C** Live cell imaging results of 72 h treatment at EC50 (concentrations noted in legend), including cell confluence (top) and fluorescent cleaved caspase 3/7+ signal area normalized to percent confluency.

DISCUSSION

In this study we explore the synergistic effect of PI3K inhibition in combination with other kinase inhibitors and drugs on merlin-deficient Schwann cells (MD-SCs) a model for specific for Neurofibromatosis type 2-associated schwannomas. The chronic nature of NF2 and its benign characteristics make it very challenging to develop reliable and successful targeted drug treatments [17]. PI3K signaling is one of the most frequently overactivated pathways in cancer. NF2 mutations lead to absent or nonfunctional merlin protein and in consequence PI3K pathway activation, making this disease a good candidate for PI3K targeted therapy [8, 18]. Moreover, loss of merlin has been shown to activate other signaling pathways, including the Ras/Raf/MEK/ERK, FAK/Src, Rac/PAK/JNK, mTORC1 and Wnt/ β -catenin [18]. We have previously shown that simultaneous inhibition of complementary pathways exposes vulnerable targets due to synergistic effects [19]. The use of high throughput viability and synergy analyses to test a large number of inhibitors was beneficial in identifying a single favorable combination that induced similar responses across a number of cell lines in multiple species. That is why we explored the synergistic effect of three PI3K inhibitors in combination with inhibitors targeting other kinases and found that the best synergy was occurred with the combination of pictilisib (pan-PI3K inhibitor) and PF-3758309 (PAK inhibitor) in human as well as in mouse MD-SCs. Pictilisib is an orally available small-molecule inhibitor for all four classes of PI3K isoforms.

Human tumor xenograft models proved its anti-tumor activity with 98% and 80% growth inhibition in glioblastoma and ovarian cancer xenografts [20]. First clinical phase 1 study proved pictilisib to be well tolerated with signs of anti-tumor activity in patients with advanced solid tumors [21]. However, PI3K inhibitors are known to have cytostatic effects rather than cytotoxic, and their impact as single agents may primarily result in tumor stabilization rather than tumor regression. Therefore, drug combination approaches have been explored. In a phase 2 FERGI study addition of pictilisib to fulvestrant for estrogen receptor positive breast cancer patients did not significantly improve progression-free survival, and dosing of pictilisib was limited by toxicity [22]. However, in another study, adding pictilisib to anastrozole significantly increased suppression of tumor cell proliferation in luminal B breast cancer [23]. Combining pictilisib with the MEK inhibitor, cobimetinib in patients with advanced solid tumors had limited tolerability and efficacy despite promising pre-clinical data [24]. Toxicity related to pictilisib and other pan-PI3K inhibitors might be dose dependent, thus studies that focus on the synergistic effect of PI3K inhibitors in combination with other drugs targeting complementary pathways may result in better tolerance and effectiveness of the treatment. In our in vivo study, we did not observe higher mice lethality in treated groups. Animals that were lost included the vehicle group and therefore we cannot attribute their loss to drug toxicity.

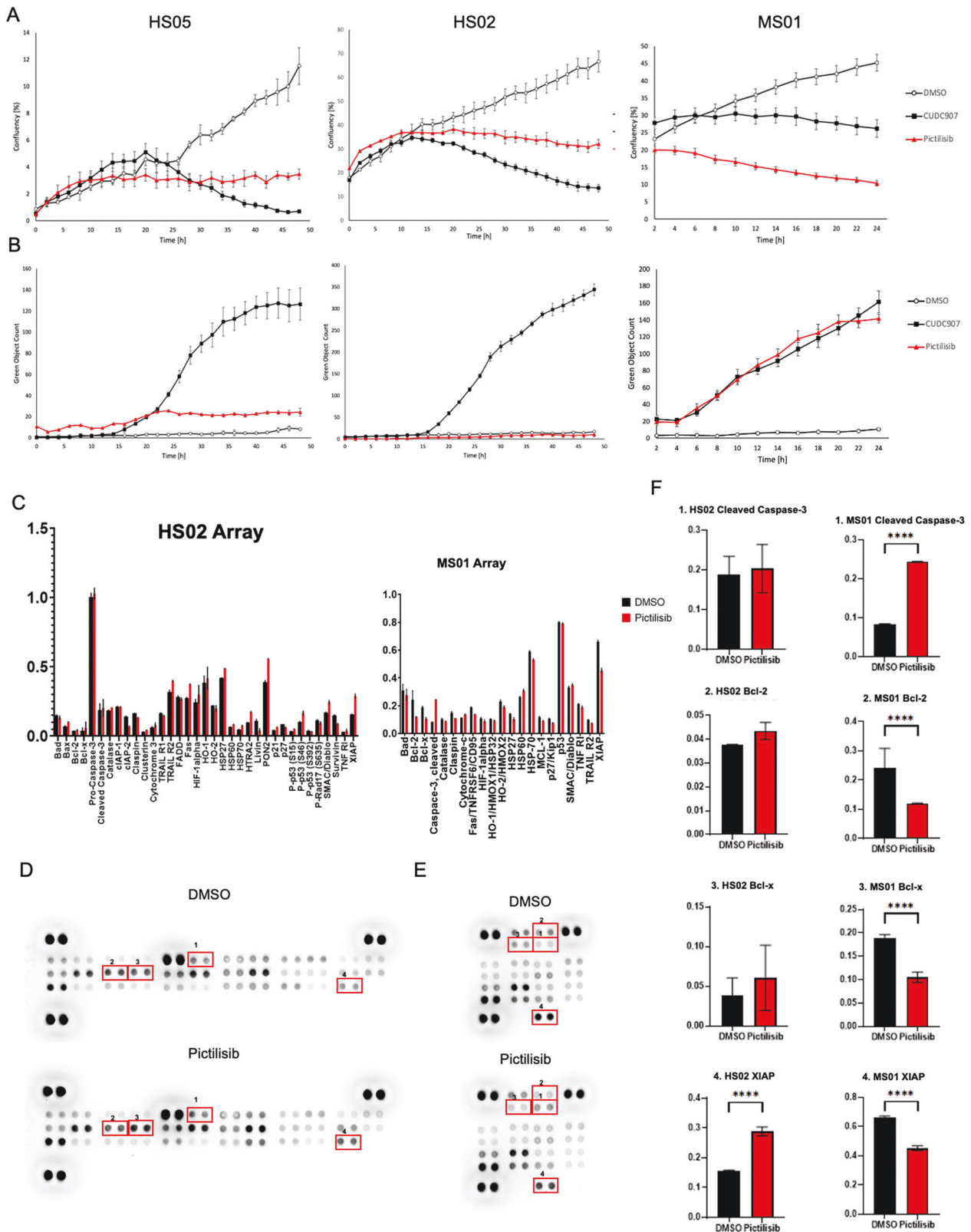


Fig. 4 Pictilisib treatment comparison in human and mouse MD-SCs. **A** Confluency measurements in two human MD-SCs (HS02 and HS05) and one mouse MD-SCs (MS01) treated with control DMSO (negative control), CUDC907 (positive control) and Pictilisib. Pictilisib significantly inhibited cell growth in all cell lines. **B** Cleaved Caspase-3/7 signals for human and mouse MD-SCs treated with Pictilisib (red) and CUDC907 (black). Pictilisib significantly induced CC-3/7 signal in mouse cells but did not in human MD-SCs. **C** Graphs presented all measured protein on apoptosis protein arrays, human on the right, mouse on the left. **D** Human Protein Profiler Apoptotic Array representative image, numbers correspond to the proteins in the graphs. **E** Mouse Protein Profiler Apoptotic Array representative image, numbers correspond to the proteins in the graphs. **F** Graphs representing protein levels detected by protein arrays, numbers correspond to the spots on the arrays; * $p < 0.05$; ** $p < 0.01$, **** $p < 0.0001$ by Šidák's multiple comparisons test.

P21-activated kinases (PAKs) are positioned at the nexus of several oncogenic signaling pathways. Schwannomas from NF2 patients were described as exhibiting PAK activation due to merlin loss [25]. Moreover, in merlin-deficient tumors the Rac/PAK pathway was described as contributing to the loss of contact inhibition and activation of WNT/ β -catenin signaling pathway [26]. Later PAK inhibitors have been shown to induce schwannoma cell death via mitotic catastrophe [27]. In our *in vivo* study the most significant decrease in tumor growth was observed with pictilisib and its use in combination treatment. We did not observe a significant difference in tumor weight between mice receiving the pictilisib monotherapy and those receiving the combination treatment. A possible explanation is that the cytotoxic effect of pictilisib is the same in both treatments and that the cytostatic effect of PF3758309 over the time course studied did not significantly contribute to tumor weight. However, combination treatment presented the most significant decrease in Ki67, pAkt, and YAP levels suggesting that it had the most comprehensive influence on the tumor. In human MD-SCs most significant inhibition observed was in cell cycle with combination treatment. However, we did not observe any cleaved caspases 3 or 7 signal that was present in mouse MD-SCs after treatment with pictilisib *in vitro* as well as in the tissue. Although some data indicates that PI3K inhibitors may induce apoptosis, for example in sarcomas [28] or HER2-positive breast cancer [29], consensus is that PI3K inhibitors mostly affect cell proliferation rather than cell survival [30]. In the *in vivo* study, we observed significantly decreased final tumor weight in the pictilisib-treated groups that were associated with caspase 3/7 activation and decreased pAKT staining. This is consistent with inhibition of PI3K activity promoting apoptosis of mouse schwannoma cells in immune deficient mice. Whether this would occur in immune competent humans with schwannomas is unknown. Prior observations in the lab suggest that mouse and human schwannoma cells are “wired” differently in relation to cell death signaling mechanisms. We find that mouse schwannoma cells undergo cell death more readily than human schwannoma cells when challenged with cytostatic agents. Therefore, we compared pictilisib-treated human and mouse MD-SCs using apoptosis antibody arrays and confirmed their different behaviors. Mouse MD-SCs undergo apoptosis with the induction of caspase 3 cleavage and Bcl-2 and Bcl-x downregulation. Human MD-SCs cells did not present with cleaved caspase 3 or downregulation of anti-apoptotic proteins with pictilisib treatment. This indicates that results of pre-clinical studies using mouse models and virally modified human schwannoma cell lines may not be predictive of sustained human responses to cytostatic drugs.

Comprehensive pharmacokinetic assessments determined the time course of the presence of drugs in blood plasma and nerve tissue suggesting drugs should be present at 4 h post-gavage. However, metabolism can vary due to a number of environmental factors [31], and detection of a drug does not always correlate with its activity. However, we demonstrated that co-treatment alters drug metabolism and increases the half-life of pictilisib in plasma, which may be a mechanism of drug synergy and explain the increased PI3K inhibition in combination treated animals. Further studies could elucidate drug activity in relation to the presence of these inhibitors during metabolism.

We idena clear reduction in YAP protein levels in grafts treated with PF-3758309 alone an in combination. The Hippo pathway plays an essential role in maintaining tissue homeostasis by regulating cell processes such as proliferation, migration, and survival. Merlin is a key upstream regulator of the Hippo kinase core protein, suppressing downstream YAP activity as a transcription factor [32]. Not surprisingly, loss of merlin leads to dysregulation of YAP activity with its co-transcription factors TAZ and TEAD [32]. The ability to block YAP/TAZ function has been of interest in treating NF2-deficient cancers [33]. A number of studies have targeted YAP association with TEAD as a specific method to

suppress its activation and role in tumor formation [34]. Our observation in this study presents a novel method through which overall YAP expression can be controlled although it was not associated cell death induction in human schwannoma cells or in the *in vivo* mouse model. Further studies are necessary to understand the multiple signaling networks undoubtedly modulated when PAK and PI3K are targeted with these compounds.

In summary, we demonstrated that targeting PAK and PI3K pathways provide synergistic activity in several models of NF2, leading to cell cycle arrest or initiation of apoptosis. A thorough understanding of the complex and intersecting molecular pathways involved could identify new targets and inhibitors to slow NF2 schwannoma disease progression. The results support the use of combinatorial treatments at potentially lower than maximally tolerated doses of monotherapies to leverage the cooperative properties of targeted inhibitors.

MATERIALS & METHODS

Cell culture

Primary human fetal Schwann cells (SC), HS11, and HS13 were acquired from SciencCell Research Laboratories (Carlsbad, CA, USA). NF2-shRNA treatment was utilized to suppress merlin expression in HS11 cells to create two merlin-deficient SC (MD-SC) lines, HS01 and HS02. The HS03 and HS05 MD-SC lines were created by CRISPR/Cas9 with NF2sg1 (sequence: AAACATCTCGTACAGTGACA, provided by Broad Institute) in HS13 cells. Development and characterization of these cell lines, including loss of merlin, was previously described [8]. Human SCs were cultured on CellBIND Corning dishes (Corning, Corning, NY, USA) in complete Schwann cell media (SCM, basal Schwann cell medium plus 5% fetal bovine serum, Schwann cell growth supplements, 100 Units/mL penicillin, and 100 μ g/mL streptomycin). Mouse MD-SCs (MTC-10) were generated and characterized in 2010 and then underwent lentiviral luciferase transduction [8, 19]. Mouse SCs were cultured on CellBIND Corning dishes in N2 medium (F12, Dulbecco’s modified Eagle medium, and 1% N2 supplement, Gibco, ThermoFisher Scientific, Waltham, MA USA). Luciferase expression was confirmed prior to *in vivo* use by Western blot. All cells were routinely tested for *mycoplasma* contamination (Look-Out Mycoplasma PCR Detection Kit; Sigma Aldrich, St Luis, MO, USA).

Cell viability and synergy analysis

Drugs used in this study are listed with their targets in Table S1. All drugs were obtained from SelleckChem (Houston, TX, USA), apart from (-)-B-Hydrastine (Santa Cruz Biotechnology, Dallas, TX, USA). Drugs were dissolved in DMSO (10 mM stock). MD-SCs were seeded in 384-well CellBind Corning plates at 1000 cells/well in phenol red-free media. After attachment, cells were treated with drugs at ten concentrations in a 10 \times 10 matrix. Mouse cells were treated for 48 h and human cells for 72 h prior to assessment of cell viability with CellTiter-Fluor Assay (Promega, Madison, WI, USA). All drugs were tested in at least two human MD-SC lines. Follow up testing was performed on a subset of combinations using the mouse MD-SC line. Matrix combination data was uploaded into the Combenefit software system to assess drug synergy using three methods (Loewe, Bliss, and HSA) [35].

Cell cycle analysis

HS01 cells were seeded at 125,000 cells/well in a 6-well CellBIND Corning plate and allowed to attach overnight. Cells were then treated with 0.001% DMSO, 2.5 μ M pictilisib, 150 nM PF-3748309, or a combination of the two drugs for 24 h. EdU (10 μ M) (Click-iT EdU kit; Molecular Probes, ThermoFisher) was added during the last 3 h. Cells were collected with 0.05% trypsin, stained with violet live/dead stain (ThermoFisher Scientific), and permeabilized. DNA labeling with FxCycle stain (ThermoFisher Scientific) was

performed according to manufacturer's instructions. Cell populations were identified by flow cytometry on CytoFlex (Beckman Coulter, Brea, CA, USA) and analyzed by CytExpert software (Beckman Coulter). Experiment was performed in three replicates.

Cell death assay (Incucyte)

Human HS11, HS01, HS02, HS13, and HS05 and mouse MTC-10 cells (1000 cells/well) were seeded in growth medium in three replicate wells/condition of a 384-well CellBIND Corning plate. After ~6 h, drugs (diluted in 0.001% DMSO) at three increasing concentrations (EC₅₀ as well as lower and higher concentrations) and Incucyte® Caspase-3/7 Green Apoptosis Assay Reagent (Sartorius, Gottingen, Germany) were added to the wells. Wells were imaged using the Incucyte® S5 Live-Cell Analysis system (Sartorius) for 24–72 h. Phase and green fluorescent images were collected every 2 h and analyzed using the integrated basic analyzer software.

Apoptosis array assay

Human HS02 MD-SCs and mouse MTC-10 (MS01) MD-SCs cell lines were used. Briefly, cells were seeded on 10 cm plates and treated with DMSO (0.001%) or pictilisib (2.5 μM) for 6 h. This time was selected based on previous Incucyte data and coincided with MTC-10 cells started to round up and detach. Cells were lysed and procedure was performed according to the Proteome Profiler Human or Mouse Apoptosis Array Kit (Cat No: ARY009 for Human, Cat No: ARY031 for Mouse, Biotechne, Minneapolis, MA, USA). Arrays were visualized using the Jess System (Biotechne), densitometry was measured in two replicate spots and normalized to the mean of six reference spots using ImageJ Software (NIH, Bethesda, MD, USA). Calculations were carried out using Prism 9 Software (GraphPad, Boston, MA, USA).

Pharmacokinetic studies

Male and female *NOD.Cg-Prkdcscid Il2rgtm1Wjl/SzJ* (NSG) mice were bred in house and all care and use was approved by the University of Central Florida (UCF) Institutional Animal Care and Usage Committee (IACUC; #19-05, approved 04/08/2019). The UCF animal facility is accredited by the Association for Assessment and Accreditation of Laboratory Animal Care. A total of 50 six- to eight-week-old mice were used for pharmacokinetic studies. Blood and sciatic nerve samples from NSG mice were collected at 1, 2, 4, 8, and 24 h after a single oral gavage of 75 mg/kg for pictilisib and 25 mg/kg for PF-3758309 both individually and combined. Drugs were delivered via 0.5% methylcellulose, 0.2% Tween 80, and 10% DMSO vehicle. Ten mice (three per drug and one control receiving vehicle alone) were used at each time point. Collected samples were frozen and sent to Cyprotex (Watertown, MA, USA) for LC-MS/MS quantitation of drug levels. Pharmacokinetic calculations were performed using the PKSolver software. The plasma half-life ($t_{1/2}$) was calculated as the time required to reduce by half the plasma concentration after reaching pseudo-equilibrium and is not the time required to eliminate half the administered dose. An additional LC-MS/MS analyses of a subset of the treated mice (see below) was conducted. This was done to determine whether PF-3758309 was accessible to the tumor neovasculature that can differ from that of the organ/tissue housing the tumor. Three mice from each treatment group were selected randomly at the end of the in vivo study to assess the levels of drug in plasma, intact control nerve, and tumor. Samples were collected 4 h after the final oral gavage, frozen, and sent to Cyprotex for analysis.

Orthotopic nerve allograft model

A total of 48 NSG mice (6 and 7 weeks old) were implanted with 5000 MS01-*Luc* cells as previously described [19, 36]. This group size was determined from past studies to be sufficient to obtain statistical significance for graft weight. Seven days post-implantation, mice were imaged with an In Vivo Imaging System (IVIS,

Perkin-Elmer, Waltham, MA, USA) and peak radiance measurements (typically 8–15 min post-injection) were used to assign mice to treatment groups ensuring even distribution of initial tumor burden and sex between groups. All mice successfully established orthotopic MS01-*Luc* allografts. Mice were dosed daily by oral gavage starting on day 8. Mice ($n = 12$ /group) received vehicle (0.5% methylcellulose, 0.2% Tween 80, 10% DMSO, pictilisib (75 mg/kg), PF-3758309 (25 mg/kg), or a combination of both treatments. Mice were imaged every 7 days and were euthanized after 14 days of treatment (4 h after last treatment). Eight mice became ill and died or were euthanized due to weight loss per IACUC protocol (final sample size (n): vehicle: 11; pictilisib: 9; PF-3758309: 12; combination: 8). Tissue from $n = 3$ mice/group was collected, frozen, and sent to Cyprotex for analysis.

Histology and immunohistochemistry

Immediately after euthanization, contralateral control nerves and grafted nerves were re-moved, weighed, and measured (maximum length and width). Grafts were placed in 4% paraformaldehyde and fixed overnight at 4 °C followed by standard paraffin processing. Samples were embedded and 5 μm sagittal sections were collected (from $n = 4$ /group). Sections were stained with hematoxylin and eosin (H&E) or used for immunohistochemistry. Slides were deparaffinized and rehydrated. Antigen retrieval reaction was performed by heating sections in Antigen Unmasking Solution (pH = 6.0, Vector Labs, Newark, CA, USA) in a 100 °C water bath for 20 min. Endogenous peroxidase activity was blocked with BLOXALL solution (Vector Labs). After blocking for 1 h with 5% normal goat serum in PBS, primary antibodies were applied and slides were incubated overnight at 4 °C. Primary antibodies used were rabbit anti-S100 (GA504; 1:200; Dako Omnis, Agilent, Santa Clara, CA, USA), rabbit anti-phospho-PAK1/2/3 (PA5-101019, S144, S141, S139; 1:120; Invitrogen, Waltham MA, USA), rabbit anti-T308pAKT (ab38449, 1:70; Abcam, Cambridge, United Kingdom), rabbit anti-Ki67 (ab16667, 1:200; Abcam) rabbit anti-cleaved caspase-3 (#9664, 1:500; Cell Signaling, Danvers, MA, USA), and rabbit anti-YAP (#14074, 1:200; Cell Signaling) Sections were then washed and the ImmPRESS HRP Anti-Rabbit IgG Polymer Detection Kit (Vector Labs) was used followed by ImmPACT DAB HRP substrate (Vector Labs) to develop a colorimetric (brown) signal. Sections were counter-stained with hematoxylin and mounted with VectraMount Permanent Mounting Medium (Vector Labs). Sections were imaged with a Keyence BZ-X810, selecting several regions of interest (ROI) from each section; images were collected at 400x magnification. Staining was quantified as percent positive area using the IHC toolbox plugin for ImageJ (NIH, v1.53e). At least two sections per sample were used for each protein target, with a minimum of 4 ROIs imaged per section to account for tissue heterogeneity.

Statistics

GraphPad Prism Version 7.04 was used for statistical analysis. One-way analysis of variance (ANOVA) was used to compare IVIS radiance fold change and tumor size between single and combination drug- and vehicle treated groups. Two-way ANOVA with Bonferroni correction was used to compare treatment groups for cell cycle analysis and violet ratiometric membrane asymmetry assay. Parametric (ANOVA) and non-parametric (Kruskal-Wallis) tests were used for immunohistochemical quantification analysis after testing for normality. Statistical significance was set at $p < 0.05$.

DATA AVAILABILITY

Data sharing not applicable to this article as no datasets were generated or analyzed during the current study.

REFERENCES

- Halliday D, Emmanouil B, Evans DGR. Updated protocol for genetic testing, screening and clinical management of individuals at risk of *NF2*-related schwannomatosis. *Clin Genet*. 2023;103:540–52.
- Bachir S, Shah S, Shapiro S, Koehler A, Mahammedi A, Samy RN, et al. Neurofibromatosis Type 2 (NF2) and the implications for vestibular schwannoma and meningioma pathogenesis. *Int J Mol Sci*. 2021;22:690.
- Kissil JL, Wilker EW, Johnson KC, Eckman MS, Yaffe MB, Jacks T. Merlin, the product of the *Nf2* tumor suppressor gene, is an inhibitor of the P21-activated kinase, Pak1. *Mol Cell*. 2003;12:841–9.
- Okada T, You L, Giancotti FG. Shedding light on Merlin's wizardry. *Trends Cell Biol*. 2007;17:222–9.
- Comes P, Peyre M, Sanson M, Sterkers O, Bernardeschi D, Kalamirides M. Current management of large vestibular schwannomas for NF2 patients in a National Reference Center. *Laryngoscope*. 2021;131:E98–107.
- Gugel I, Grimm F, Tatagiba M, Schuhmann MU, Zipfel J. Management of neurofibromatosis type 2 and schwannomatosis associated peripheral and intraspinal schwannomas: influence of surgery, genetics, and localization. *J Neurooncol*. 2022;159:271–9.
- Ghalavand MA, Asghari A, Farhadi M, Taghizadeh-Hesary F, Garshasbi M, Falah M. The genetic landscape and possible therapeutics of neurofibromatosis type 2. *Cancer Cell Int*. 2023;23:99.
- Petrilli AM, Fernández-Valle C. Role of Merlin/NF2 inactivation in tumor biology. *Oncogene*. 2016;35:537–48.
- Sekido Y. Inactivation of Merlin in malignant mesothelioma cells and the Hippo signaling cascade dysregulation. *Pathol Int*. 2011;61:331–44.
- Arakawa H, Hayashi N, Nagase H, Ogawa M, Nakamura Y. Alternative splicing of the *NF2* gene and its mutation analysis of breast and colorectal cancers. *Hum Mol Genet*. 1994;3:565–8.
- Evans DGR. Neurofibromatosis type 2 (NF2): a clinical and molecular review. *Orphanet J Rare Dis*. 2009;4:16.
- Petrilli AM, Fuse MA, Donnan MS, Bott M, Sparrow NA, Tondera D, et al. A chemical biology approach identified PI3K as a potential therapeutic target for neurofibromatosis type 2. *Am J Transl Res*. 2014;6:471–93.
- Allaway R, Angus SP, Beauchamp RL, Blakeley JO, Bott M, Burns SS, et al. Traditional and systems biology based drug discovery for the rare tumor syndrome neurofibromatosis type 2. *PLoS One*. 2018;13:e0197350.
- Huegel J, Dinh CT, Martinelli M, Bracho O, Rosario R, Hardin H, et al. CUDC907, a dual phosphoinositide-3 kinase/histone deacetylase inhibitor, promotes apoptosis of NF2 Schwannoma cells. *Oncotarget*. 2022;13:890–904.
- Nussinov R, Tsai CJ, Jang H. A new view of pathway-driven drug resistance in tumor proliferation. *Trends Pharm Sci*. 2017;38:427–37.
- Mayer IA, Arteaga CL. The PI3K/AKT pathway as a target for cancer treatment. *Annu Rev Med*. 2016;67:11–28.
- Querdani A, Goutagny S, Kalamirides M, Trocóniz IF, Ribba B. Mechanism-based modeling of the clinical effects of bevacizumab and everolimus on vestibular schwannomas of patients with neurofibromatosis type 2. *Cancer Chemother Pharm*. 2016;77:1263–73.
- Zhou L, Hanemann CO. Merlin, a multi-suppressor from cell membrane to the nucleus. *FEBS Lett*. 2012;586:1403–8.
- Fuse MA, Plati SK, Burns SS, Dinh CT, Bracho O, Yan D, et al. Combination therapy with *c-Met* and *Src* inhibitors induces caspase-dependent apoptosis of merlin-deficient schwann cells and suppresses growth of schwannoma cells. *Mol Cancer Ther*. 2017;16:2387–98.
- Raynaud FI, Eccles SA, Patel S, Alix S, Box G, Chackowree I, et al. Biological properties of potent inhibitors of class I phosphatidylinositol 3-kinases: from PI-103 through PI-540, PI-620 to the oral agent GDC-0941. *Mol Cancer Ther*. 2009;8:1725–38.
- Sarker D, Ang JE, Baird R, Kristeleit R, Shah K, Moreno V, et al. First-in-Human Phase I Study of Pictilisib (GDC-0941), a Potent Pan-Class I Phosphatidylinositol-3-Kinase (PI3K) Inhibitor, in Patients with Advanced Solid Tumors. *Clin Cancer Res*. 2015;21:77–86.
- Krop IE, Mayer IA, Ganju V, Dickler M, Johnston S, Morales S, et al. Pictilisib for oestrogen receptor-positive, aromatase inhibitor-resistant, advanced or metastatic breast cancer (FERGI): a randomised, double-blind, placebo-controlled, phase 2 trial. *Lancet Oncol*. 2016;17:811–21.
- Schmid P, Pinder SE, Wheatley D, Macaskill J, Zammit C, Hu J, et al. Phase II randomized preoperative window-of-opportunity study of the PI3K inhibitor pictilisib plus anastrozole compared with anastrozole alone in patients with estrogen receptor-positive breast cancer. *J Clin Oncol*. 2016;34:1987–94.
- Shapiro GI, LoRusso P, Kwak E, Pandya S, Rudin CM, Kurkjian C, et al. Phase Ib study of the MEK inhibitor cobimetinib (GDC-0973) in combination with the PI3K inhibitor pictilisib (GDC-0941) in patients with advanced solid tumors. *Invest N. Drugs*. 2020;38:419–32.
- Yi C, Wilker EW, Yaffe MB, Stemmer-Rachamimov A, Kissil JL. Validation of the p21-activated kinases as targets for inhibition in neurofibromatosis type 2. *Cancer Res*. 2008;68:7932–7.
- Zhou L, Ercolano E, Ammoun S, Schmid MC, Barczyk MA, Hanemann CO. Merlin-deficient human tumors show loss of contact inhibition and activation of Wnt/ β -catenin signaling linked to the PDGFR/*Src* and *Rac*/*PAK* pathways. *Neoplasia*. 2011;13:1101–IN2.
- Mercado-Pimentel ME, Miller C, Rolph DN, Villalobos EF, Dunn AM, Mohan PM, et al. Inhibiting p21-activated kinase induces cell death in vestibular schwannoma and meningioma via mitotic catastrophe. *Otol Neurotol*. 2017;38:139–46.
- Isoyama S, Tamaki N, Noguchi Y, Okamura M, Yoshimatsu Y, Kondo T, et al. Subtype-selective induction of apoptosis in translocation-related sarcoma cells induced by PUMA and BIM upon treatment with pan-PI3K inhibitors. *Cell Death Dis*. 2023;14:169.
- Will M, Qin ACR, Toy W, Yao Z, Rodrik-Outmezguine V, Schneider C, et al. Rapid Induction of Apoptosis by PI3K Inhibitors Is Dependent upon Their Transient Inhibition of RAS-ERK Signaling. *Cancer Discov*. 2014;4:334–47.
- Vanhaesebroeck B, Perry MWD, Brown JR, André F, Okkenhaug K. PI3K inhibitors are finally coming of age. *Nat Rev Drug Discov*. 2021;20:741–69.
- Vinarov Z, Abdallah M, Agundez JAG, Allegaert K, Basit AW, Braeckmans M, et al. Impact of gastrointestinal tract variability on oral drug absorption and pharmacokinetics: an UNGAP review. *Eur J Pharm Sci*. 2021;162:105812.
- Harvey KF, Zhang X, Thomas DM. The Hippo pathway and human cancer. *Nat Rev Cancer*. 2013;13:246–57.
- Sato T, Sekido Y. NF2/Merlin inactivation and potential therapeutic targets in mesothelioma. *Int J Mol Sci*. 2018;19:988.
- Tang TT, Konradi AW, Feng Y, Peng X, Ma M, Li J, et al. Small molecule inhibitors of TEAD auto-palmitoylation selectively inhibit proliferation and tumor growth of NF2-deficient mesothelioma. *Mol Cancer Ther*. 2021;20:986–98.
- Di Veroli GY, Fornari C, Wang D, Mollard S, Bramhall JL, Richards FM, et al. Combeneft: an interactive platform for the analysis and visualization of drug combinations. *Bioinformatics*. 2016;32:2866–8.
- Turk AN, Byer SJ, Zinn KR, Carroll SL. Orthotopic xenografting of human luciferase-tagged malignant peripheral nerve sheath tumor cells for in vivo testing of candidate therapeutic agents. *J Vis Exp*. 2011;49:2558.

ACKNOWLEDGEMENTS

We thank Peggy Wallace for sharing the primary adult human schwann cells used to create HS04.3 and Stephen Lambert for critical comments on the manuscript. The UCF vivarium staff for training and assistance with mouse study.

AUTHOR CONTRIBUTIONS

CFV conceived the project. JH, AP, RR, BV, and CFV designed the experiments. CFV supervised the experiments. AN, JH, AP, RR, BV, and HH performed experiments and collected data. AN, JH, AP, RR, HH, and CFV analyzed the data. AN, JH, AP, HH, and CFV interpreted the results. AN, JH, and CFV wrote the initial draft followed by input and edits from all authors. All authors have read and agreed to the published version of the manuscript.

FUNDING

This research was funded by the State of Florida Department of Health Live Like Bella Initiative, grant number 8LA02 and R56NS102254 to CFV.

COMPETING INTERESTS

The authors declare no competing interests.

ADDITIONAL INFORMATION

Supplementary information The online version contains supplementary material available at <https://doi.org/10.1038/s41388-024-02958-w>.

Correspondence and requests for materials should be addressed to Cristina Fernandez-Valle.

Reprints and permission information is available at <http://www.nature.com/reprints>

Publisher's note Springer Nature remains neutral with regard to jurisdictional claims in published maps and institutional affiliations.



Open Access This article is licensed under a Creative Commons Attribution 4.0 International License, which permits use, sharing, adaptation, distribution and reproduction in any medium or format, as long as you give appropriate credit to the original author(s) and the source, provide a link to the Creative Commons licence, and indicate if changes were made. The images or other third party material in this article are included in the article's Creative Commons licence, unless indicated otherwise in a credit line to the material. If material is not included in the article's Creative Commons licence and your intended use is not permitted by statutory regulation or exceeds the permitted use, you will need to obtain permission directly from the copyright holder. To view a copy of this licence, visit <http://creativecommons.org/licenses/by/4.0/>.

© The Author(s) 2024